THE JOURNAL OF BIOLOGICAL CHEMISTRY
Vol. 280, No. 8, Issue of February 25, pp. 7088–7099, 2005

Printed in U.S.A.

The Structural and Dynamic Basis of Ets-1 DNA Binding Autoinhibition*[S]

Received for publication, September 17, 2004, and in revised form, December 3, 2004
Published, JBC Papers in Press, December 9, 2004, DOI 10.1074/jbc.M410722200

Gregory M. Lee‡§, Logan W. Donaldson‡§¶, Miles A. Pufall‖, Hyun-Seo Kang‡, Isabelle Pot‡, Barbara J. Graves‖, and Lawrence P. McIntosh‡**

From the ‡Department of Biochemistry and Molecular Biology, Department of Chemistry, and The Biotechnology Laboratory, University of British Columbia, Vancouver, British Columbia V6T 1Z3, Canada and the ‖Department of Oncological Sciences, Huntsman Cancer Institute, University of Utah, Salt Lake City, Utah 84112

The transcription factor Ets-1 is regulated by the allosteric coupling of DNA binding with the unfolding of an α-helix (HI-1) within an autoinhibitory module. To understand the structural and dynamic basis for this autoinhibition, we have used NMR spectroscopy to characterize Ets-1ΔN301, a partially inhibited fragment of Ets-1. The NMR-derived Ets-1ΔN301 structure reveals that the autoinhibitory module is formed predominantly by the hydrophobic packing of helices from the N-terminal (HI-1, HI-2) and C-terminal (H4, H5) inhibitory sequences, along with H1 of the intervening DNA binding ETS domain. The intramolecular interactions made by HI-1 in Ets-1ΔN301 are similar to the intermolecular contacts observed in the crystal structure of an Ets-1ΔN300 dimer, confirming that the latter represents a domain-swapped species. ^{15}N relaxation studies demonstrate that the backbone of the N-terminal inhibitory sequence is mobile on the nanosecond-picosecond and millisecond-microsecond time scales. Furthermore, hydrogen exchange measurements reveal that amide protons in helices HI-1 and HI-2 exchange with water at rates only ~15- and ~75-fold slower, respectively, than predicted for an unfolded polypeptide. These findings indicate that inhibitory helices are only marginally stable even in the absence of DNA. The energetic coupling of DNA binding with the facile unfolding of the labile HI-1 provides a mechanism for modulating Ets-1 DNA binding activity via protein partnerships, post-translational modifications, or mutations. Ets-1 autoinhibition illustrates how conformational equilibria within structural domains can regulate macromolecular interactions.

Gene expression can be controlled by modulating the DNA binding affinity of sequence specific transcription factors. Similar to several other transcription factors, the DNA binding of Ets-1 is modulated by an autoinhibitory module that provides a route to biological regulation (1). The Ets-1 inhibitory module is composed of sequences flanking the winged helix-turn-helix (HTH)[1] DNA binding ETS domain (2, 3). When these sequences are deleted, as in an alternatively spliced isoform of Ets-1, or when their structural elements are disrupted by mutations, as in the case of the oncogenic v-Ets, the affinity of Ets-1 for its target DNA sites is enhanced by 10- to 20-fold (4–6). In a cellular context, this module is essential for response to different regulatory signals. DNA binding of Ets-1 is enhanced 10- to 20-fold through a partnership with the transcription factor RUNX1 (CBFα2/AML1) (7). Conversely, in activated T-cells, phosphorylation of a serine-rich region (residues 244–300) inhibits the DNA binding of Ets-1 by another ~50-fold (8). Importantly, these two effects require an intact inhibitory module.

Mechanistic insight into autoinhibition has come from the observation that the Ets-1 inhibitory module changes conformation upon binding to DNA. Initial secondary structural studies performed in our laboratories demonstrated that this module is composed of four coupled α-helices, located N- terminal (HI-1, HI-2) and C-terminal (H4, H5) to the ETS domain (Fig. 1*A*). Chemical shift data from NMR spectra comparing an inhibited fragment, Ets-1ΔN280,[2] to one missing the N-terminal inhibitory sequences, Ets-1ΔN331, mapped the contacts of HI-1 and HI-2 to the first helix of the ETS domain (H1) and to the C-terminal inhibitory region near H4 and H5 (9, 10). This implicated helix H1 in the autoinhibitory mechanism due to its role in both directly contacting DNA and in packing of the inhibitory helices (11). Importantly, these contacts also lie on a contiguous surface of the protein opposite the DNA recognition helix (H3), indicating that autoinhibition does not result from a simple steric blockage of DNA binding. Instead, limited proteolysis and CD spectroscopic studies revealed that HI-1 unfolds upon complex formation with DNA (2, 3). Together, these data led to the proposal that autoinhibition results from the allosteric coupling of a helix-coil transition with DNA binding, and that the affinity of Ets-1 for DNA is inversely correlated with the stability of the inhibitory module.

* This work was supported by grants from the National Cancer Institute of Canada with funds from the Canadian Cancer Society (to L. P. M.), the National Institutes of Health Grants GM38663 (to B. J. G.) and CA24014 (to the Huntsman Cancer Institute), and CA93247 and GM08537 for training grant support (to M. A. P.). The costs of publication of this article were defrayed in part by the payment of page charges. This article must therefore be hereby marked "*advertisement*" in accordance with 18 U.S.C. Section 1734 solely to indicate this fact.

The atomic coordinates of the Ets-1ΔN301 ensemble (code 1R36) have been deposited in the Protein Data Bank, Research Collaboratory for Structural Bioinformatics, Rutgers University, New Brunswich, NJ (http://www.rcsb.org/).

The NMR chemical shift list (accession code 5991) has been deposited in the BioMagResBank at www.bmrb.wisc.edu/.

[S] The on-line version of this article (available at http://www.jbc.org) contains Supplemental Materials.

§ Both authors contributed equally to this work.

¶ Present address: Dept. of Biology, York University, Toronto, ON M3J 1P3, Canada.

** A CIHR Scientist. To whom correspondence should be addressed. Tel.: 604-822-3341; Fax: 604-822-5227; E-mail: mcintosh@otter.biochem.ubc.ca.

[1] The abbreviations used are: HTH, helix-turn-helix; CD, circular dichroism; HSQC, heteronuclear single quantum correlation; HX, hydrogen exchange; NOE, nuclear Overhauser effect; NOESY, nuclear Overhauser effect spectroscopy; pH*, the observed pH meter reading without correction for isotope effects; RDC, residual dipolar coupling; r.m.s.d., root mean-square deviation; PDB, Protein Data Bank.

[2] Ets-1 fragments are indicated by the boundaries of truncations from the N terminus of the protein, *e.g.* Ets-1ΔN301 is a deletion of residues 1–300 and corresponds to Ets-1(301–440).

X-ray crystallographic studies have extended the framework for understanding the autoinhibition phenomenon. A crystal structure of Ets-1ΔN280 in complex with DNA demonstrated that helix HI-1 is disordered, whereas HI-2, H4, and H5 are coupled and contact the core ETS domain via H1 (12). The crystal structure of a second, partially inhibited fragment, Ets-1ΔN300, solved in the absence of DNA, showed a conformation similar to bound Ets-1ΔN280, but with a folded HI-1 (12). Ets-1ΔN300, however, crystallized as a dimer, with HI-1 of one subunit interfaced with HI-2, H4, and H5 of an adjacent subunit.[3] This dimeric state was not expected, and indeed, subsequent mutagenic analyses suggested that the *in trans* position of HI-1 in this crystal approximated its *in cis* position in the monomeric protein in solution. Thus, Ets-1ΔN300 appeared to crystallize as a three-dimensional domain-swapped dimer (13). Both of these structures also displayed features of the ETS domain-DNA interface similar to those observed in several investigations of related Ets proteins (14–17), including the role of H3 in major groove binding and direct sequence recognition, along with the involvement of H1 in a hydrogen-bonded phosphate contact (11, 18, 19).

Although these extensive structural and functional studies have laid a foundation for understanding the mechanism of autoinhibition, several key questions remained unanswered. What is the structure of the inhibitory module in the unbound state of the native Ets-1 monomer? What are the features of HI-1 that allow a facile helix-coil transition, and does this transition occur even in the absence of DNA? Finally, what couples DNA binding to the inhibitory action of helices that lie distant from the recognition helix of the ETS domain?

To address these questions, we have studied the partially-inhibited Ets-1ΔN301 in its DNA-free form using NMR spectroscopy. Our findings yielded the first high-resolution structure of a monomeric Ets-1 fragment that displays the intramolecular packing of all inhibitory helices. In parallel, backbone amide ^{15}N relaxation and hydrogen exchange data for Ets-1ΔN301 demonstrate that HI-1 is only marginally stable and thus poised to unfold. Additional regions of this protein, including the DNA binding interface, also display conformational mobility suggestive of a role in the allosteric mechanism of autoinhibition.

EXPERIMENTAL PROCEDURES

Sample Preparation—The gene encoding Ets-1ΔN301 (residues 301–440 of murine Ets-1) was constructed by ligation of a PCR-amplified NdeI/EcoRI fragment of the wild-type *ets*-1 gene (corresponding to residues 301–352) with an EcoRI/HindIII fragment of a synthetic, codon-biased *ets*-1 gene into pET22b (Invitrogen). The final Ets-1ΔN301 construct encoded an additional Met and Gly at its N terminus, and unless stated otherwise, a surface C416S substitution to help limit oxidative cross-linking. This mutation causes minimal NMR spectral, and by inference, structural perturbations (data not shown). Ets-1ΔN301 was purified as described previously (2, 9, 20) from soluble extracts of *Escherichia coli* HMS174(λDE3) grown at 37 °C in M9 minimal medium supplemented with the following: 1 gm/liter (^{15}N, 99%)-NH_4Cl for uniform ^{15}N labeling; 1 gm/liter (^{15}N, 99%)-NH_4Cl and 3 gm/liter ($^{13}C_6$, 99%)-glucose for uniform $^{13}C/^{15}N$ labeling; 1 gm/liter (^{15}N, 99%)-NH_4Cl, 3 gm/liter ($^{13}C_6$, 99%)-glucose, and 1 g/liter (^2H, 97%; ^{13}C 98%, ^{15}N, 98%)-Celtone powder (Spectra Stable Isotopes) in 95% ^2H_2O for uniform $^2H/^{13}C/^{15}N$ labeling; and 0.3 gm/liter ($^{13}C_6$, 99%)-glucose and 2.7 gm/liter ($^{12}C_6$)-glucose for non-random 10% ^{13}C-labeling (21). Ets-1ΔN301, selectively labeled with ring-deuterated aromatic amino acid residues, was prepared in synthetic rich medium containing two of ($^2H_5$-$\gamma^{1,2}$,$\delta^{1,2}$,ζ)-Phe, ($^2H_4$-$\gamma^{1,2}$,$\delta^{1,2}$)-Tyr, or ($^2H_5$-δ^1,ζ^1,ζ^2,ϵ^3,η^2)-Trp (Cambridge Isotope Laboratories) (22). A similar approach was used to selectively label Ets-1ΔN301 with $^{13}C^{\beta}$-Ala. Electrospray ionization mass spectrometry and Edman sequencing of purified Ets-1ΔN301 confirmed that the N-terminal Met was absent.

NMR Spectral Assignments—NMR experiments were performed on Varian Unity 500 MHz, Inova 600 MHz, and Inova 800 MHz spectrometers. Spectra were acquired at 28 °C with protein concentrations ranging from 0.3–0.8 mM in an NMR sample buffer containing 20 mM sodium phosphate (pH 6.5), 500 mM NaCl, 5 mM dithiothreitol, 0.02% NaN_3, and ~10% D_2O. The high ionic strength was critical for protein solubility. Spectral processing and analysis were performed using Felix 2000 (Accelrys, Inc.), NMRPipe (23), and Sparky (24).

Assignments of the Ets-1ΔN301 backbone and side chain ^1H, ^{13}C, and ^{15}N resonances were obtained using an extensive set of multidimensional NMR experiments (25) acquired on protein samples uniformly ^{15}N-, $^{15}N/^{13}C$-, or $^2H/^{15}N/^{13}C$-labeled, as well as selectively labeled with $^{13}C^{\beta}$-Ala or with ring-deuterated Tyr, Phe, or Trp. Full assignments of only nine residues, located within the HI-1/HI-2 loop (Lys^{318}, Pro^{319}, Ile^{321}, Pro^{322}), HI-2 (Ala^{323}, Thr^{330}), H3 (Tyr^{397}, Asp^{398}), and between H3 and S3 (Lys^{399}) were not obtained because of exchange broadening and/or spectral overlap. Stereochemical assignments of the signals from non-degenerate β-methylene protons (37 of 104 possible) were based upon HNHB and short mixing time ^{15}N-TOCSY-HSQC (τ_m = 38 ms) experiments, while those of side chain Gln and Asn amide protons (7 of 8 pairs) were obtained from an EZ-HMQC-NH_2 spectrum (26). Complete stereochemical assignments of the Val and Leu methyl group resonances were determined from a constant time ^1H-^{13}C HSQC spectrum acquired on a non-randomly 10% ^{13}C-labeled sample (21).

Structure Calculations—Structural calculations were performed using ARIA/CNS version 1.2 with torsional angle dynamics (27, 28). NOE restraints were determined from a ^1H-^{15}N-^1H NOESY-HSQC (τ_m = 100 ms) recorded on ^{15}N-labeled Ets-1ΔN301; a ^{15}N-^{15}N-^1H NOESY-HSQC (τ_m = 200 ms) recorded on $^2H/^{13}C/^{15}N$-labeled Ets-1ΔN301; and a simultaneous ^1H-$^{15}N/^{13}C$-^1H NOESY-HSQC (τ_m = 100 ms) focused on aliphatic side chains, a ^1H-^{13}C-^1H NOESY-HSQC (τ_m = 100 ms) for aromatic side chains, and a simultaneous constant time methyl ^{13}C-$^{13}C/^{15}N$-^1H NOESY (τ_m = 140 ms), all recorded on a uniformly $^{13}C/^{15}N$-labeled protein sample in H_2O buffer (29). Most NOE cross-peaks were manually picked and assigned prior to intensity calibration in ARIA.

Backbone dihedral angles were determined from C^{α}, C^{β}, C′, H^{α}, and H^N chemical shifts using TALOS (30). The χ_1 side chain dihedral angles for residues with β-methylene protons were determined from a conservative examination of short mixing time ^{15}N TOCSY-HSQC (τ_m = 38 ms) and HNHB spectra, according to a staggered rotomer model. Side chain χ_1 dihedral angles for Ile, Val, and Thr residues were derived on the basis of $^3J_{NC\gamma}$ and $^3J_{C'C\gamma}$ coupling constants measured from ^{13}C-{^{15}N} and ^{13}C-{$^{13}C'$} spin echo difference CT-HSQC spectra (31). All Xaa-Pro amides were constrained to the trans conformation, based upon their proline $^{13}C^{\alpha}$ chemical shifts (32), as well as the absence of (Xaa)H^{α}-(Pro)H^{α} interactions in NOESY spectra. The charge states of the His imidazoles were not experimentally determined and thus were set to the default fully protonated form. A limited set of hydrogen bond restraints were included for amides located in helices or strands, as determined via NOE and chemical shift information and protection from hydrogen-deuterium exchange.

Residual dipolar couplings (RDCs) were acquired on a uniformly ^{15}N-labeled protein sample diffused into a 5% acrylamide gel (29:1 acrylamide:bisacrylamide stock) (33). The gel was cast at a 6 mm diameter and ~20 mm length, dialyzed against NMR sample buffer, and soaked in a solution containing labeled protein overnight, giving a calculated final Ets-1ΔN301 concentration of ~0.1–0.2 mM. Prior to spectral acquisition, the pellets were loaded into a 5-mm silanized bottomless NMR tube using a gel stretching apparatus (34) purchased from New Era Enterprises, Inc. The gel stretched ~2.1 times its original length, yielding splittings of ~5 Hz in a ^2H-NMR spectrum of the $^1HO^2H$ lock solvent. Backbone ^1H-^{15}N RDCs were measured from the ^1H-^{15}N-IPAP-HSQC spectrum (35) of the partially aligned protein, relative to that of a reference spectrum recorded for unaligned Ets-1ΔN301. 49 RDC restraints, ranging from −17.8 to +11.5 Hz for amides in the helical and β-sheet regions of Ets-1ΔN301 with well resolved NMR signals, were used for the structural calculations. Axial and rhombic parameters were estimated using a histogram method, followed by a grid search to determine the optimal values of D_a (−8.9 Hz) and R (0.3) resulting in minimal SANI violations during the final energy minimization step of ARIA/CNS (36).

The Ets-1ΔN301 structure ensemble was calculated using a two-step ARIA protocol. An initial round of ARIA (it0 → it8), starting with an unfolded polypeptide, was completed with only dihedral angle and hydrogen bond restraints and uncalibrated NOE data. A second full ARIA calculation (it1 → it8) followed, with RDC restraints included, using the prefolded structures and the unambiguous and ambiguous

[3] Coordinates of a similar crystal dimer structure have been deposited with PDB accession code 1GVJ.

NOE restraint sets from the previous round as the starting parameters. A total of 50 structures were calculated per iteration during each round, of which the energetically top 25 from the final iteration were further refined in a water box using Lennard-Jones potentials. The ARIA-derived unambiguous and ambiguous NOE distance restraints were evaluated using VMD-Xplor (37). Analyses of the structures were performed using MolMol (38), InsightII (Accelrys, Inc.), and Procheck-NMR (39). Secondary structure boundaries for the ensemble were defined according to Promotif (40) and Vadar (41).

NMR Relaxation Measurements—Amide ^{15}N relaxation parameters for ^{15}N-labeled Ets-1ΔN301 were acquired on a 500 MHz spectrometer at 28 °C using water-selective pulse sequences (42). Data points for the T_1 (11, 56, 122, 200, 333, 522, 788, and 1066 ms) and T_2 (17, 33, 50, 67, 84, 100, 117, and 150 ms) experiments were collected in random order with one duplicate each to facilitate error analysis. Steady-state heteronuclear $^1H\{^{15}N\}$-NOE spectra were acquired with and without 3 s of ^1H saturation and a total recycle delay of 5 s. Relaxation rates and extended anisotropic Lipari-Szabo model-free relaxation parameters (43–45) were calculated using Curvefit (46) and Tensor2 (47), respectively. Based on the average minimized structure, the global motions of Ets-1ΔN301 were fit to a fully anisotropic diffusion tensor with D_{ZZ} = 1.82 (± 0.04) × 10^7 s^{-1}, D_{YY} = 1.67 (± 0.03) × 10^7 s^{-1}, and D_{XX} = 1.65 (± 0.04) × 10^7 s^{-1}; this approximates a slightly prolate ellipsoid with $D_\parallel/D_\perp$ ~1.1 ± 0.05. The resulting model-free parameters are tabulated in Supplemental Table SI.

Amide ^{15}N relaxation-dispersion parameters for Ets-1ΔN301 were acquired with relaxation-compensated ^1H-^{15}N CPMG-HSQC experiments recorded using 600 MHz and 800 MHz NMR spectrometers (48). The constant time CPMG-T_2 delays were set to 40 msec, whereas spectra corresponding to the effective B_1 fields, υ_{CPMG} (600 MHz: 50, 100, 150, 200, 300, 400, 500, 600, 700, 800, 900, and 1000 Hz; 800 MHz: 50, 100, 150, 200, 250, 300, 350, 400, 500, 600, 700, 800, 900, and 1000 Hz), were collected in random order with three duplicate data points. Relaxation-dispersion parameters were calculated from a fit of R_2^{eff} *versus* υ_{CPMG} using a Matlab (The MathWorks, Inc.) module provided by O. Millet (49).

Amide Hydrogen Exchange—Slow amide proton-deuterium exchange rates (28 °C, pH* 6.5) were measured from a series of sensitivity-enhanced ^1H-^{15}N HSQC spectra recorded after rapid transfer of wild type ^{15}N-labeled Ets-1ΔN301 through a Sephadex G-25 spin column equilibrated with NMR sample buffer prepared in 99% D_2O (50). The first spectrum, started ~8 min. after transfer, was acquired in 11 min, while subsequent spectra were recorded with increasing numbers of transients per t1 increment for improved signal-to-noise. After scaling according to the number of transients, pseudo-first order rate constants for exchange, k_{ex}, were obtained by least squares fitting of peak intensity, I_t, *versus* the mid-point time of each spectrum to the equation $I_t = I_o\exp(-k_{ex}t) + I_\infty$, where I_∞ accounts for the effect of residual protonated water (~5%).

Rapid amide proton-proton exchange rates at 28 °C and pH 6.86 to 8.25 were determined for wild-type ^{15}N-labeled Ets-1ΔN301 by the CLEANEX-PM method (51) using a series of 6 spectra with transfer periods ranging from 10 to 60 msec. Each spectrum was recorded in ~5 h using a recycle delay of 2.05 s. Reference spectra were recorded in ~5 h using a recycle delay of 12.1 s to ensure complete relaxation. For improved signal-to-noise, duplicated data sets were measured and merged at both pH 7.50 and 7.74. Pseudo-first order rate constants for chemical exchange, k_{ex}, were obtained by least squares fitting of peak intensities to published equations (51), using a Matlab module provided by W.-Y. Choy (University of Toronto) and assuming a negligible contribution from water relaxation.

Predicted exchange rates, k_{pred}, for an unstructured polypeptide with the sequence of Ets-1ΔN301 were calculated with the program Sphere (52) using poly-DL-alanine reference data corrected for amino acid type, pH, temperature, and isotope effects (53, 54).

RESULTS

Spectral Assignments of Ets-1ΔN301—This NMR study was performed on Ets-1ΔN301, a truncation fragment of Ets-1 spanning residue 301 to its native C terminus. The affinity of Ets-1ΔN301 for a consensus DNA sequence is ~2-fold inhibited relative to Ets-1ΔN331, the fully de-repressed fragment lacking the entire N-terminal inhibitory sequence, as compared with ~10-fold for both Ets-1ΔN280 and full-length Ets-1 (data not shown). Thus, although retaining all of the inhibitory helices (Fig. 1*A*), Ets-1ΔN301 is only partially-inhibited due to the absence of residues 280–300. While essential for full repression (2), these residues are conformationally disordered (9) and their deletion substantially improved the amenability of the resulting Ets-1ΔN301 toward detailed NMR spectroscopic studies.

Nearly complete backbone and side chain ^1H, ^{13}C, and ^{15}N resonance assignments of Ets-1ΔN301 were obtained through a suite of $^1H/^{13}C/^{15}N$ scalar and NOE-correlated experiments (Fig. 1*B*). Critical to this process was uniform ^2H isotopic labeling, which helped to enhance spectral sensitivity and resolution. Selective ^2H isotopic labeling of aromatic residues also aided in the resonance assignments of their side chain nuclei, while selective $^{13}C^\beta$-alanine labeling of Ets-1ΔN301 facilitated analysis of the poorly resolved signals from ^{323}AAALA^{328} within the N-terminal inhibitory region. These extensive assignments permitted the detailed structural and dynamic analyses of Ets-1ΔN301.

NMR-based Structure Determination of Ets-1ΔN301—The tertiary structure of Ets-1ΔN301 was calculated with ARIA/CNS (27, 28) using manually-picked NOE peak lists from an extensive set of three-dimensional ^{15}N- and ^{13}C-resolved NOESY spectra. Calculations also included backbone and side chain dihedral angles, along with a limited set of hydrogen bond and ^1H-^{15}N RDC restraints corresponding to residues within elements of regular secondary structure. A summary of the refinement statistics for the energetically best 25 final structures is listed in Table I, and a plot of backbone and side chain r.m.s.d. values is given in Supplemental Fig. S1.

In agreement with previous NMR spectroscopic and x-ray crystallographic analyses (9, 12), the calculated Ets-1ΔN301 structure ensemble consists of seven α-helices (HI-1: residues 304–310, HI-2: 323–330, H1: 337–346, H2: 368–378, H3: 386–398, H4: 418–422, H5: 426–432) and four anti-parallel β-strands (S1: 354–356, S2: 362–365, S3: 402–405, S4: 411–414). The distorted single-turn H4 was observed, but not explicitly defined as a helix in our earlier NMR studies of Ets-1ΔN280 and Ets-1ΔN331 (9, 10). The ETS domain, residues 331–415, folds as a winged HTH composed of a three-helix bundle and a four-stranded, anti-parallel β-sheet. Helices H2 and H3 form the HTH motif, whereas the β-strands provide the "wing" for this well characterized DNA binding domain. The NMR-derived Ets-1ΔN301 ETS domain structure superimposes well with the corresponding region of the crystallographically determined Ets-1ΔN300 structure (12). A comparison of the solution structure ensemble over residues 331–415 with the corresponding crystallographic coordinates (PDB accession code 1MD0) yields r.m.s.d. values of 1.7 ± 0.1 and 1.3 ± 0.1 Å between all backbone atoms and those contained within helices and strands, respectively. Minor differences between the structures lie primarily within flexible exposed regions, such as the turn of the HTH motif and the S3/S4 β-hairpin loop.

The Ets-1ΔN301 structural ensemble extends previous studies by providing the first picture of the intramolecular packing between the autoinhibitory module and the ETS domain. The N- and C-terminal inhibitory helices (HI-1, HI-2, H4, and H5) are structurally coupled to one another and pack with the first helix (H1) of the ETS domain (Fig. 2, *A* and *B*). The N-terminal inhibitory helix, HI-1, lies approximately anti-parallel to HI-2, parallel to H1 and H5, and abuts H4 in a tail-to-head fashion. This tertiary packing is consistent with comparisons of the HSQC spectra of Ets-1ΔN280 and Ets-1ΔN331 (9) and of Ets-1ΔN301 and Ets-1ΔN331 (data not shown), which reveal significant amide chemical shift perturbations (*i.e.* $\Delta\delta > 0.1$ ppm for ^1H) for residues within H1 and the C-terminal inhibitory sequence because of the presence of the N-terminal inhibitory sequence. In contrast, the chemical shifts of amides within the remainder of the ETS domain correspond more closely between

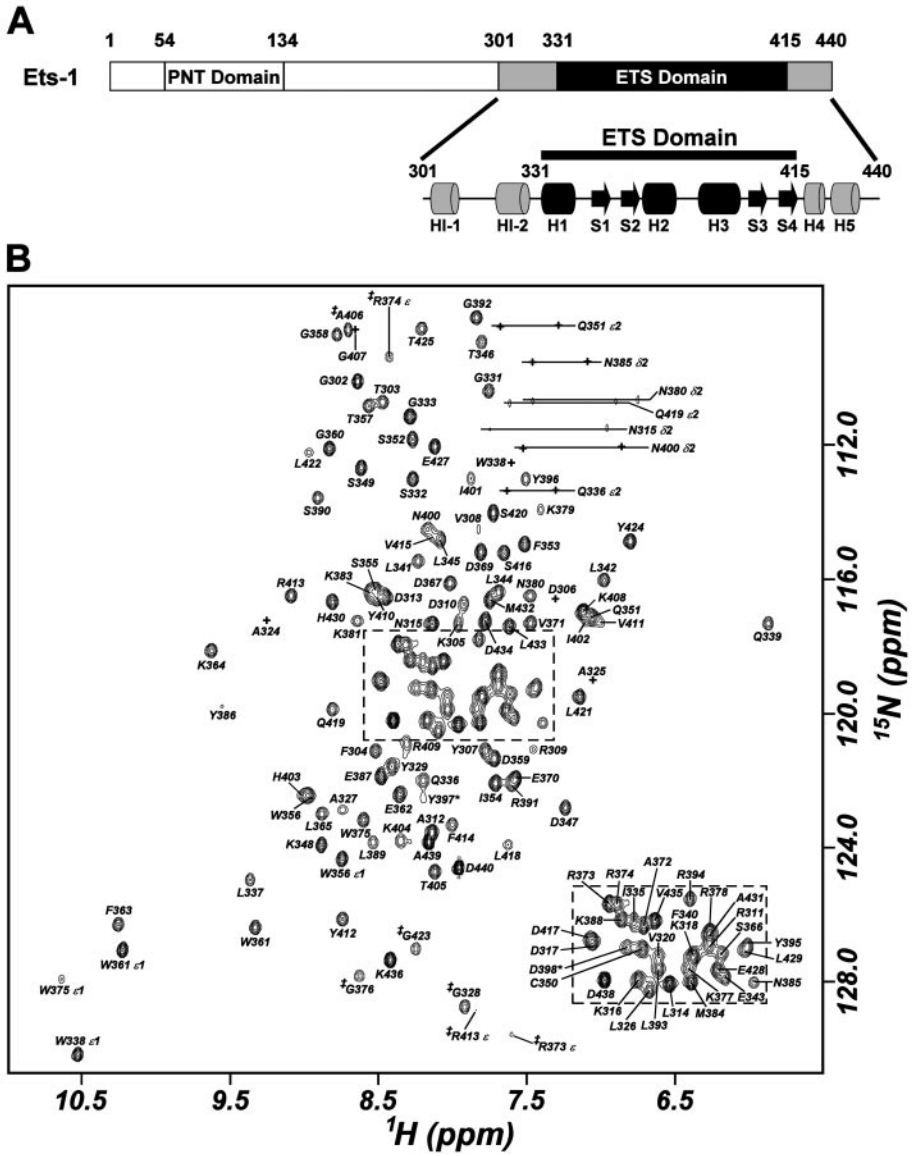

FIG. 1. *A*, secondary structure of Ets-1ΔN301 in context of full-length Ets-1. The ETS domain (*black*) is composed of three α-helices (H1, H2, H3), and four β-strands (S1, S2, S3, S4), while the inhibitory module (*gray*) includes two N-terminal (HI-1, HI-2) and two C-terminal (H4, H5) helices. Multiple phosphorylation of a serine-rich region (residues 244–300) reinforces autoinhibition (8). The PNT domain, which serves as an ERK2 docking site (74, 75), has no apparent role in DNA binding. *B*, assigned ^{1}H-^{15}N HSQC spectrum of murine Ets-1ΔN301 (pH 6.5, 28 °C). The *inset* corresponds to the crowded region at the center of the spectrum. Aliased peaks (‡), tentative assignments (*), and weak peaks not observed at this contour level (+) are indicated. The signals from Asn and Gln side chain $^{15}NH_2$ groups are suppressed because of the use of a refocused INEPT within this HSQC pulse sequence.

the two fragments, indicating that the inhibitory module, located on the opposite face of the molecule, does not markedly perturb the structure of the winged HTH DNA binding motif.

An extensive network of hydrophobic interactions stabilizes the inhibitory module. This network is composed mainly of non-polar side chains of residues in HI-1 (Phe^{304}, Tyr^{307}, Val^{308}), the HI-1/HI-2 loop (Ala^{312}, Leu^{314}, Pro^{319}, Val^{320}, Ile^{321}, Pro^{322}), HI-2 (Ala^{323}, Ala^{324}, Ala^{325}, Leu^{326}, Ala^{327}, Gly^{328}, Tyr^{329}, Thr^{330}), the HI-2/H1 loop (Ile^{335}), H1 (Trp^{338}, Phe^{340}, Leu^{342}, Thr^{346}), H4 (Leu^{418}, Leu^{421}, Leu^{422}), the H4/H5 loop (Tyr^{424}), H5 (Leu^{429}, Met^{432}), and near the C terminus (Leu^{433}) (Fig. 2, *C* and *D*). Of particular note, Phe^{304} and, to a lesser extent, Tyr^{307} and Val^{308} connect the amphipathic HI-1 (^{304}FKDYVRD^{310}) to regions in the N- and C-terminal inhibitory module, specifically, residues within the HI-1/HI-2 loop (Ala^{312}, Leu^{314}, Pro^{319}, Val^{320}, Ile^{321}, Pro^{322}), HI-2 (Ala^{325}, Leu^{326}, Tyr^{329}), H4 (Leu^{422}), and the H4/H5 loop (Tyr^{424}). Remarkably similar intermolecular interactions involving these three hydrophobic residues from helix HI-1 are observed in the Ets-1ΔN300 crystal structure (12), indicating that the salient features of the crystalline dimer model closely reflect the intramolecular packing of the inhibitory module in solution. Residues within the HI-1/HI-2 loop (^{319}PVIP^{322}) and the hydrophobic HI-2 (^{323}AAALAGYT^{330}) also help establish the integrity of this module through van der Waals packing against atoms within the N- and C-terminal inhibitory regions, as well as H1 of the ETS domain. In a reciprocal manner, several large hydrophobic residues within the H4-loop-H5 region (Leu^{422}, Tyr^{424}, and Leu^{429}) contribute to the core of the inhibitory module by interacting with side chains from HI-1, HI-2, H1, and the HI-1/HI-2 loop. Also integral to the inhibitory module structure are residues within H1 (Trp^{338}, Phe^{340}, Leu^{342}, and Thr^{346}). This network of non-polar groups within the inhibitory module closely resembles that observed in the Ets-1ΔN300 crystal structure (12). The only noteworthy structural differences are observed near the C-terminal end of HI-1 and the start of the HI-1/HI-2 loop (^{311}RADLNKDK^{318}). This segment adopts a relatively extended conformation in the crystal dimer, running antiparallel with respect to its counterpart, to serve as an intermolecular bridge between the two monomer subunits. Conversely, the same sequence packs against the inhibitory helices in the solution structure of monomeric Ets-1ΔN301.

The inhibitory module structural ensemble also exhibits several notable polar interactions. First, HI-1 and H4 lie in a skewed tail-to-head arrangement at an angle of 50.3° ± 2.5°, such that the N terminus of HI-1 directly abuts the C terminus of H4 (Fig. 2, *A* and *B*), likely allowing a favorable interaction between the two helical macrodipoles. Furthermore, based on

TABLE I
NMR restraints and structural statistics for the Ets-1ΔN301 ensemble

Summary of restraints	
NOEs: unambiguous (ambiguous) ARIA restraints	
Intraresidue	1004 (27)
Sequential	667 (73)
Medium range ($1 < \|i-j\| < 5$)	474 (83)
Long range ($\|i-j\| \geq 5$)	1123 (354)
Total	3268 (537)
Dihedral angles	
ϕ,ψ, χ_1	93, 93, 51
Hydrogen bonds	40 × 2
Residual dipolar couplings	49
Deviation from restraints	
NOE restraints, Å	0.0573 ± 0.0012
Dihedral restraints, degree	1.16 ± 0.05
Residual dipolar coupling restraints, Hz	0.72 ± 0.03
Residues in allowed regions of Ramachandran plot[a]	98.5%
Deviation from idealized geometry	
Bonds, Å	0.0049 ± 0.00012
Angles, degree	0.65 ± 0.01
Improper angles, degree	1.83 ± 0.06
Mean energies, kcal-mol^{-1}	
E_{vdw}	−405.11 ± 15.57
E_{bonds}	55.92 ± 2.84
E_{angle}	268.42 ± 10.73
E_{impr}	161.60 ± 8.42
E_{NOE}	341.03 ± 15.95
E_{cdih}	19.42 ± 1.80
E_{sani}	25.17 ± 1.99

r.m.s.d. from average structure	Ets domain 331–415	Residues 301–436
Backbone (N, Cα, C′), Å	0.29 ± 0.05	0.35 ± 0.05
All heavy atoms, Å	0.68 ± 0.05	0.71 ± 0.05

[a] Calculated from Procheck-NMR (39).

NOE interactions involving surrounding residues, potential carbonyl oxygen-amide nitrogen hydrogen bonds between Leu^{421} and Phe^{304} and between Leu^{422} and Lys^{305} in these two helices are consistently observed in the calculated Ets-1ΔN301 structure ensemble. Strikingly, in the crystalline Ets-1ΔN300 dimer model, HI-1 of one monomer and H4 of the other appear to form a continuous helix, with a bend of 18.6°± 0.8°, that is also stabilized by hydrogen bonds between Leu^{421}-Phe^{304} and Leu^{422}-Lys^{305}. Second, in addition to this helix-helix stacking, the Lys^{305} and Glu^{428} side chains appear to link HI-1 and H5 via a potential salt bridge observed within many members of the NMR-derived Ets-1ΔN301 structure ensemble (Fig. 2*C*). A similar intermolecular electrostatic interaction is also found in the crystalline Ets-1ΔN300 dimer. Finally, Lys^{316} and Lys^{318} in the HI-1/HI-2 loop may form salt bridges with Glu^{343} and Asp^{347}, respectively, along helix H1. These later interactions are not observed in the crystal dimer due to the role of this loop as an intermolecular bridge.

In conclusion, the NMR-derived structure of Ets-1ΔN301 defines the fold and stabilizing interactions of the native monomeric form of Ets-1 inhibitory module. The intramolecular packing of helix HI-1 with the other inhibitory helices is consistent with experimental data regarding the architecture and function of the inhibitory module (2, 3, 9, 11, 18). Furthermore, the similarities between the intramolecular interactions in Ets-1ΔN301 and the intermolecular interactions in crystalline Ets-1ΔN300 validate the proposal that the latter represents a three-dimensional domain-swapped dimer with the *in trans* position of HI-1 recapitulating its *in cis* position in a monomeric state (12, 13).

Helix HI-1 Unfolds in the Ets-1ΔN301/DNA Complex—The mechanism of DNA binding autoinhibition is proposed to involve the unfolding of inhibitory helix HI-1. The hypothesis was developed based on the observed increase in the susceptibility of Ets-1 to tryptic cleavage at the C terminus of HI-1 (Arg^{309} and Arg^{311}) and a loss of α-helical signal in its CD spectrum upon binding to DNA (2, 3). In support of this model, residues 280–308 are disordered in the crystal structure of the Ets-1ΔN280/DNA complex, whereas residues 310–318 have poorly defined electron density (12). To further investigate this conformational transition in solution, we prepared a complex of Ets-1ΔN301 and a 16-bp DNA duplex encoding a high affinity binding site. NMR-monitored titrations of Ets-1ΔN301 with this DNA confirmed that a tight 1:1 complex formed in the slow-exchange regime relative to the chemical shift time scale (data not shown).

DNA binding dramatically alters the NMR spectrum of Ets-1ΔN301. Although not assigned, the ^{1}H-^{15}N HSQC spectrum of the Ets-1ΔN301/DNA complex (Supplemental Fig. S2) reveals well-dispersed amide resonances that can be attributed to the folded ETS domain by way of comparison with data reported for a minimal-sized (residues 320–415) human Ets-1 ETS domain/DNA complex (55). However, the spectrum also contains resonances with poorly resolved amide chemical shifts characteristic of a random coil polypeptide that are not observed with uncomplexed Ets-1ΔN301. Furthermore, these amides exhibit low heteronuclear ^{1}H{^{15}N}-NOE values indicating that they are conformationally mobile on the sub-nanosecond time scale (44). In contrast, a study of selectively ^{15}N-Tyr-labeled Ets-1ΔN331 demonstrated that Tyr^{424}, which lies in the C-terminal inhibitory region, is not perturbed upon DNA binding (56). These results support the model that HI-1 is predominantly unfolded in the Ets-1ΔN301/DNA complex, whereas the C-terminal inhibitory helices are intact. The susceptibility of HI-2 toward cleavage by chymotrypsin increases in the presence of DNA, suggesting that it may become at least transiently unfolded (57). However, because of the lack of spectral assignments for DNA-bound Ets-1ΔN301, we are unable to determine if the conformation of HI-2 is also perturbed or if it remains folded, as observed in the Ets-1ΔN280/DNA crystal complex.

Dynamic Properties of Ets-1 ΔN301—The fully assigned HSQC spectrum of Ets-1ΔN301 provided an opportunity to further investigate the dynamic properties of the inhibitory helices in the absence of DNA. The modest ~10- and ~2-fold inhibition of DNA binding by Ets-1 and Ets-1ΔN301, respectively, predicts that the helix-coil transition of the N-terminal inhibitory region is relatively facile. A corollary of this prediction is that helix HI-1 is only marginally stable, even in the absence of DNA. To test these hypotheses, ^{15}N heteronuclear relaxation, relaxation-dispersion, and backbone amide hydrogen exchange measurements were performed to investigate the dynamic properties of Ets-1ΔN301.

(*a*) ^{15}N Heteronuclear Relaxation: To investigate the global hydrodynamic properties and fast time scale internal dynamics of Ets-1ΔN301, ^{15}N T_1 and T_2 lifetimes and steady-state ^{1}H{^{15}N}-NOE values were measured for 125 of the 132 backbone amides in this protein (Fig. 3*A*) (42, 44). Excluding amides exhibiting anomalous T_1/T_2 ratios or ^{1}H{^{15}N}-NOE values indicative of internal mobility, the average T_1 and T_2 lifetimes measured at a ^{1}H frequency of 500 MHz were 598 ± 31 ms and 82 ± 8 ms, respectively. These values correspond to an effective correlation time of 9.7 ± 0.05 ns for the global tumbling of Ets-1ΔN301, confirming that this 16.3 kDa protein is monomeric in solution (58). After consideration of anisotropic diffusion, the internal dynamic properties of the Ets-1ΔN301 backbone can be described by the extended Lipari-Szabo model-free formalism in terms of a generalized order parameter, S^2, which decreases from 1 to 0 with decreasing spatial restriction of the NH bond vector, as well as by additional terms including those accounting for the effects of slower conformational exchange

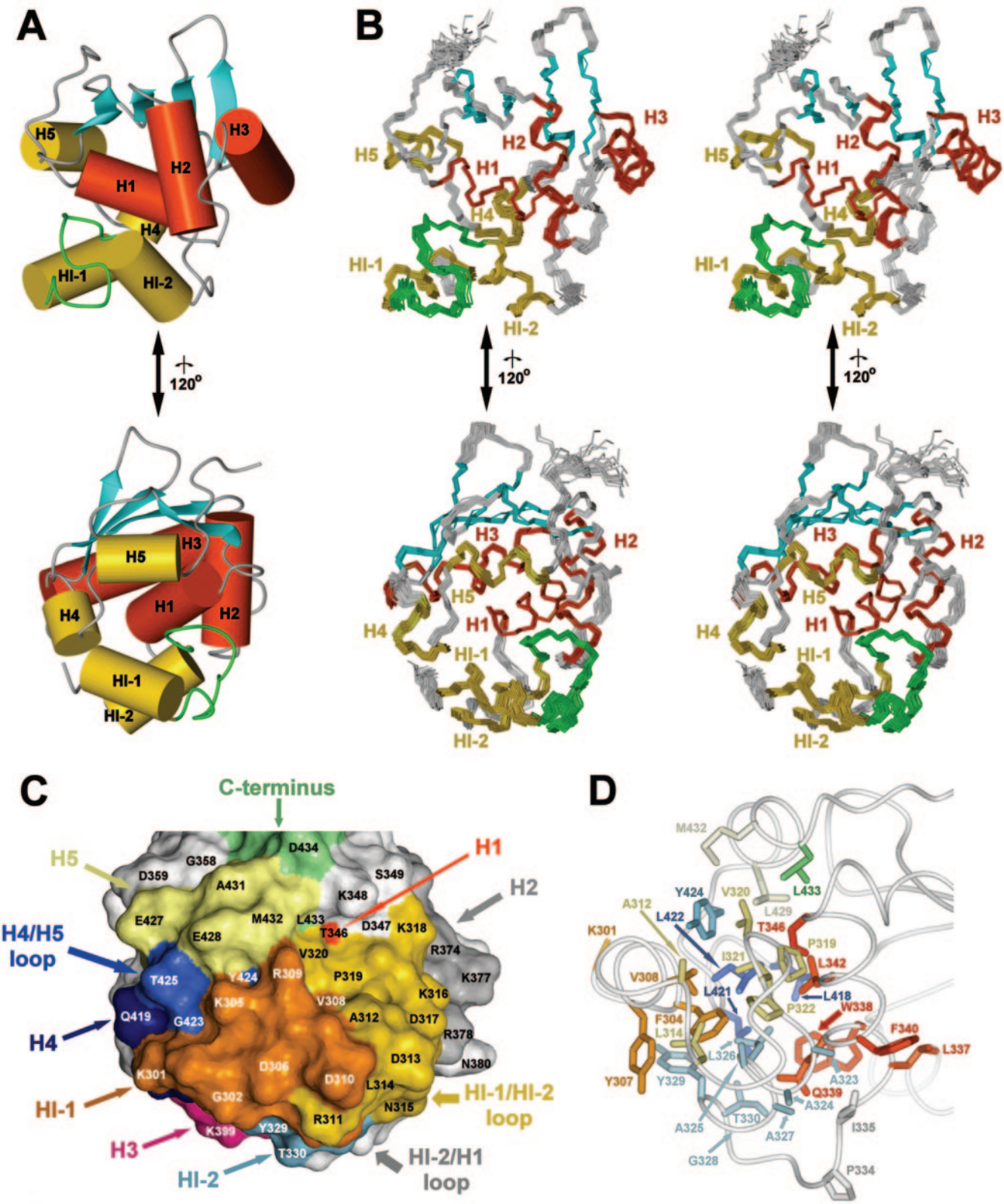

FIG. 2. **The NMR-derived structural ensemble of DNA-free Ets-1ΔN301.** Shown are the average water-refined structure (*A*) and a stereo view of the backbone of the 25 energetically best Ets-1ΔN301 structures (*B*), superimposed over the ETS domain (residues 331–415). The α-helices and winged β-sheet of the ETS domain are indicated in *red* and *cyan*, respectively, while the inhibitory helices in *gold* and the highly flexible loop between HI-1 and HI-2 in *green*. The lower figures are rotated 120° about the vertical axis relative to the upper figures. The orientation of H5 with respect to the ETS domain is reversed from that initially calculated for the NMR-derived Ets-1ΔN331 structure (PDB accession code 1ETC) because of misinterpretations of the poorly resolved spectra of the latter protein recorded with a 500 MHz spectrometer (56). *C*, surface view of the average Ets-1ΔN301 water-refined structure, focusing on the inhibitory module. Residues from HI-1 are indicated in *orange*, HI-2 in *cyan*, H1 in *red*, H4 in *dark blue*, and H5 in *light yellow*. The loop between HI-1 and HI-2 is displayed in *gold*, whereas the loop linking H4 and H5 is colored *blue*. Note that as drawn, the DNA binding interface, centered on the H2-turn-H3 motif, is on the backside of Ets-1ΔN301. *D*, *ribbon diagram* showing primarily the side chains contributing to the hydrophobic core of the inhibitory module. The coloring corresponds to that of *panel C*, while the molecule is rotated left about the vertical axis by ~90°. The figures were generated with MolMol (38).

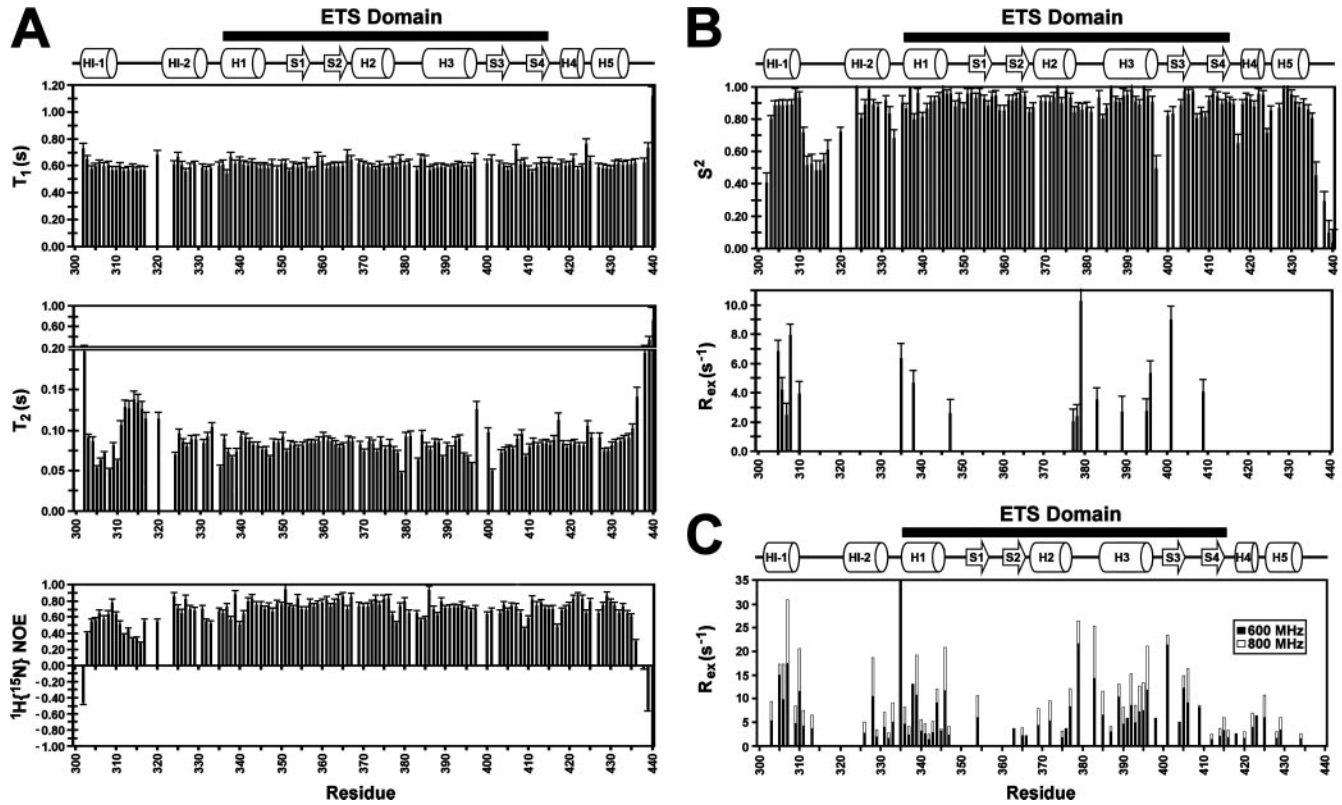

FIG. 3. **^{15}N relaxation data for Ets-1ΔN301.** *A*, backbone amide ^{15}N T_1, T_2, and heteronuclear ^{1}H{^{15}N}-NOE relaxation profile acquired at 28 °C with a 500 MHz NMR spectrometer. Longer T_2 and smaller NOE values, indicative of sub-nanosecond backbone motions, are observed for the both N and C termini, as well as the loop region between HI-1 and HI-2. Anomalously short T_2 values observed for residues in HI-1 are characteristic of conformational exchange broadening on a millisecond-microsecond time scale. Residues with missing relaxation data include prolines and amides that display overlapped or significantly weakened signals in the ^{1}H-^{15}N HSQC spectrum. *B*, fit anisotropic model-free S^2 and R_{ex} parameters. Fast internal motions are detected for the HI-1/HI-2 loop region and the N and C termini, as indicated by reduced S^2 values. Significant R_{ex} contributions to the transverse relaxation rate, $1/T_2$, because of millisecond-microsecond time scale motions are observed primarily for HI-1 and the turn of the HTH motif. *C*, backbone ^{15}N relaxation-dispersion profile acquired at magnetic fields corresponding to ^{1}H frequencies of 600 MHz (*solid bars*) and 800 MHz (*open bars*). Residues within the inhibitory module, as well as in helix HI and the DNA binding interface of the ETS domain, display R_{ex} contributions to transverse relaxation, indicating that these regions are conformationally flexible on a millisecond-microsecond time scale. As expected for conformational exchange broadening, these R_{ex} terms are larger when measured at higher magnetic fields.

broadening (R_{ex}) (43, 45, 47). The fit S^2 and R_{ex} values are presented in Fig. 3*B*, and all model-free terms tabulated within Supplemental Table SI. The relatively uniform relaxation parameters and S^2 values for the α-helices and β-strands in Ets-1ΔN301 indicate that the inhibitory module and ETS domain behave as a single, well-folded globular entity.

Local differences in the ^{15}N relaxation parameters measured for Ets-1ΔN301 reveal diversity in backbone mobility between different regions of the molecule. Within the N-terminal inhibitory sequence, two segments exhibit ^{15}N relaxation properties indicative of local dynamic properties that are distinct from the average behavior of Ets-1ΔN301 (Fig. 3, *A* and *B*). First, the amides of residues Arg^{311}-Val^{320} in the exposed loop between HI-1 and HI-2 display significantly longer T_2 times, smaller heteronuclear NOEs, and, hence, reduced S^2 values (average 0.57 ± 0.10), than those of the protein core. These data indicate that this sequence exhibits fast backbone motions on the nanosecond to picosecond time scale. This loop also has higher relative backbone r.m.s.d. values (0.44 ± 0.19 Å) relative to the more ordered regions (0.22 ± 0.09 Å) within the Ets-1ΔN301 solution structure ensemble (Fig. 2 and Supplemental Fig. S1). The flexibility of this exposed polypeptide segment is consistent with its ability to serve as an intermolecular bridge within the crystalline Ets-1ΔN300 domain-swapped dimer. Second, although the ^{1}H{^{15}N}-NOE and S^2 values (average 0.90 ± 0.03) of amides within HI-1 indicate that this helix is well-ordered on a sub-nanosecond time scale, the T_2 lifetimes measured for Lys^{305}-Asp^{310} are anomalously short. This relaxation behavior, which typically arises from a contribution of conformational exchange broadening (R_{ex}) to the overall rate of nitrogen transverse relaxation, suggests that HI-1 undergoes intermediate time scale (millisecond-microsecond) motions. This mobility, characterized further by relaxation dispersion measurements discussed below, demonstrates that even in the absence of DNA, HI-1 is conformationally dynamic relative to the remaining elements of secondary structure forming the inhibitory module and ETS domain.

Detailed inspection of the model-free analysis results for the Ets-1ΔN301 ETS domain and the C-terminal inhibitory sequence (Fig. 4*B*) also reveals reduced order parameters for amides within turns or loops (average S^2 = 0.79 ± 0.14) relative to those in helices or β-strands (0.92 ± 0.05). This expected behavior, indicative of enhanced backbone motions on the nanosecond-picosecond time scale, is particularly noteworthy for residues near the Ets-1 DNA binding interface, specifically those preceding H1, in the turn of the HTH motif, and in the H3/S3 and S3/S4 loops. A similar pattern of elevated amide nitrogen thermal factors (B values) is observed for these residues in the Ets-1ΔN300 crystallographic coordinates. Furthermore, a comparable profile of local backbone mobility was detected in an ^{15}N relaxation analysis of the related PU.1 ETS domain (59).

(*b*)^{15}N Relaxation Dispersion: To further characterize intermediate time scale (millisecond-microsecond) motions of helix HI-1 revealed by the model-free analysis, ^{15}N relaxation-dispersion measurements were performed at two static magnetic

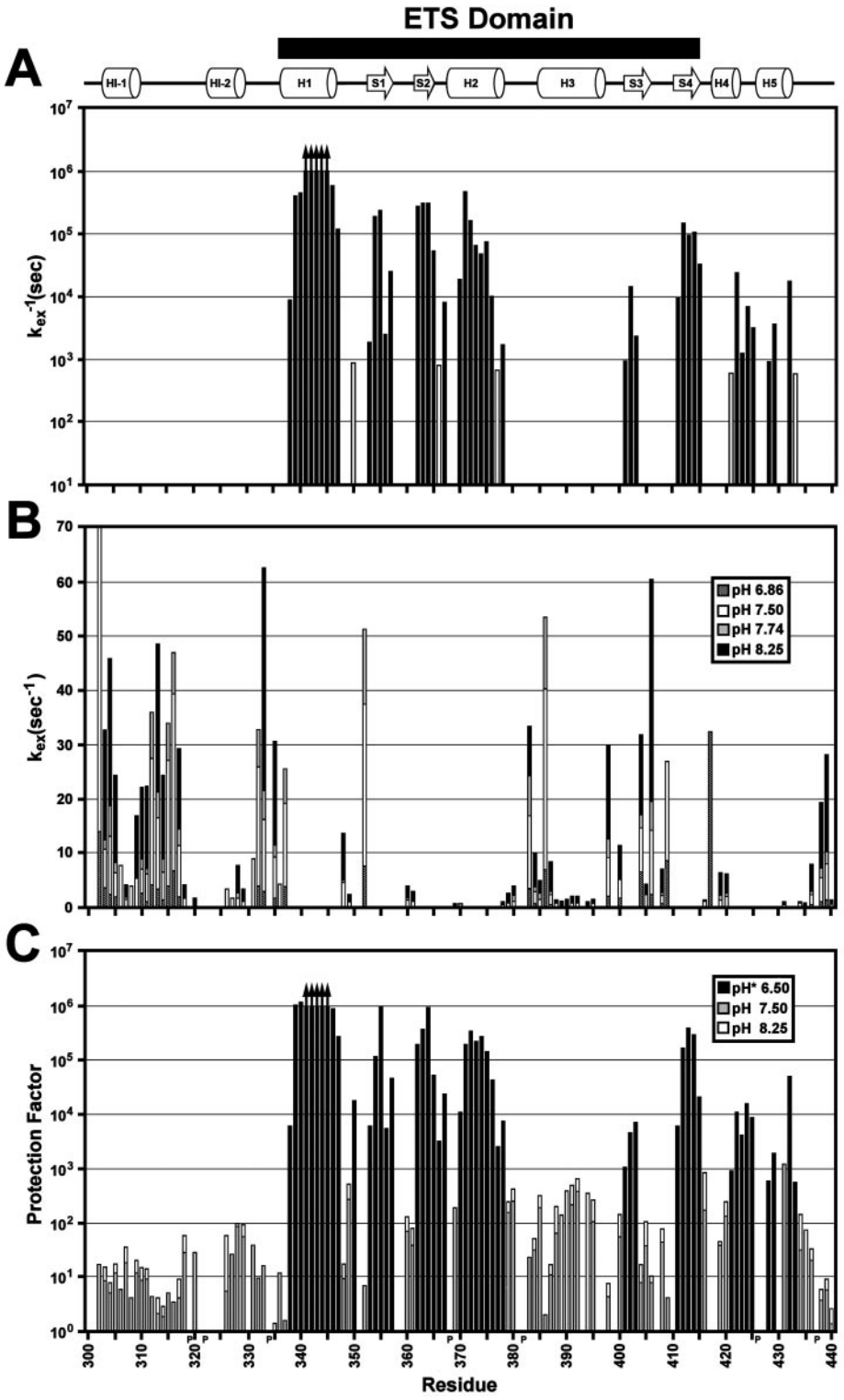

FIG. 4. **Summary of the amide HX kinetic data for wild-type Ets-1ΔN301 at 28 °C.** *A*, lifetimes ($1/k_{ex}$) for slow proton-deuterium exchange (pH* 6.5), plotted according to residue number. *Up arrows* indicate the most protected amides for which insufficient exchange occurred over the course of the 10-day experiment to allow a reliable determination of their k_{ex} values; for these residues, $1/k_{ex} > 10^6$ s. *Open bars* mark amides for which signals were observed only in the first few spectra recorded after transfer to D_2O buffer and thus $1/k_{ex} \sim 750$ s. The exchange kinetics of amides with lifetimes shorter than this limit could not be determined using this approach. *B*, rate constants, k_{ex}, for rapid proton-proton exchange measured by the CLEANEX approach at pH 6.86, 7.50, 7.74, and/or 8.25. The increase of k_{ex} with pH indicates that exchange occurs via base catalysis in the EX2 regime (62). The exchange kinetics of amides with $k_{ex} < 0.5\ s^{-1}$ could not be determined by this method. *C*, HX protection factors (k_{pred}/k_{ex}) derived using k_{ex} values measured by proton-deuterium (pH* 6.50, *black bar*) or proton-proton (pH 7.50, *gray bar*, and/or 8.25, *white bar*) exchange and predicted k_{pred} values for an unstructured polypeptide with the sequence of Ets-1ΔN301 under the corresponding experimental conditions. The small variation of protection factors with pH indicates that exchange is not exactly first order in [OH^-], likely because of pH-dependent changes in the stability or electrostatic properties of Ets-1ΔN301. Residues without protection factors are either prolines (P) or have weak or overlapping amide ^1H-^{15}N HSQC signals, thus precluding reliable HX measurements.

field strengths. These measurements sensitively detect the contribution of conformational exchange to the effective decay of transverse ^{15}N signal (48, 60). As summarized in Fig. 3*C*, signals corresponding to 115 backbone amides in Ets-1ΔN301 were collected and processed. Consistent with the anomalously short ^{15}N T_2 lifetimes measured for amides within HI-1, significant relaxation dispersion R_{ex} contributions were detected for this segment of the inhibitory module. The agreement of these complementary experimental approaches strongly indicates that in DNA-free Ets-1ΔN301, the backbone of helix HI-1 is conformationally mobile within the millisecond-microsecond time regime. Importantly, conformational exchange broadening was also detected by the relaxation-dispersion measurements for amides within the remainder of the inhibitory module (HI-2, and to a lesser extent, H4 and H5), as well as in helix H1 of the ETS domain with which they are interfaced. Furthermore, residues forming the DNA binding surface of Ets-1, including the turn of the HTH motif, the recognition helix H3, the loop following H3, and the S3/S4 loop also exhibited R_{ex} terms. These measurements reveal that the backbone of the Ets-1ΔN301 DNA binding interface, as well as the inhibitory module, undergo motions on a millisecond-microsecond time scale.

Further evidence for these motions lies with the observation of anomalously weak ^{1}H-^{15}N HSQC peaks from residues in both the inhibitory module (Asp^{306}, Val^{308}, Arg^{309}, Lys^{318}, Ile^{321}, Ala^{323}, Ala^{324}, Ala^{325}, Ala^{327}, Thr^{330}, Leu^{418}, Leu^{422}) and the ETS domain (Trp^{338}, Lys^{379}, Tyr^{386}, Tyr^{397}, Asp^{298}, Lys^{399}, Ile^{401}) of Ets-1ΔN301 (Fig. 1*B*). Together, these relaxation data suggest that regions of Ets-1ΔN301 beyond helix HI-1 are also in a conformational equilibrium in the absence of DNA.

(*c*) Amide Hydrogen Exchange: As a complementary approach, amide hydrogen exchange (HX) studies were undertaken to probe the stability and dynamics of DNA-free Ets-1ΔN301. The rate at which an amide hydrogen exchanges with water depends on its structural and electrostatic environment, as well as conformational fluctuations allowing contact with the solvent. Of primary importance are those motions involving the disruption of backbone hydrogen bonds, such as those in regular secondary structural elements (61). According to standard models of protein HX in the pH-dependent EX2 regime, the protection factor for a given amide, defined as the ratio of its predicted exchange rate in a random coil polypeptide, k_{pred}, to its measured value in a folded protein, k_{ex}, can be interpreted as the inverse of an equilibrium constant describing fluctuations between a closed, non-exchangeable state and a transiently exposed, exchange-competent state (62). Thus protection factors provide a measure of the residue-specific free energy changes ($\Delta G^{o}_{HX} = RT\ln(k_{pred}/k_{ex})$) governing local or global conformational equilibria allowing exchange.

Slow proton-deuterium HX rate constants measured for Ets-1ΔN301 are summarized in Fig. 4*A*. As observed previously for Ets-1ΔN331 (20) and Ets-1ΔN280 (9), hydrogen-bonded amides within all of the α-helixes and β-strands of the ETS domain, except surprisingly H3, were significantly protected from exchange. The slowest exchanging amides are located in H1, suggesting that this helix forms the most stable core of the protein. With protection factors $>10^6$ for these amides (Fig. 4*C*), the free energy for the global unfolding of Ets-1ΔN301 under native conditions is >8 kcal/mol. Amides in helices H4 and H5 and the intervening H4/H5 loop showed moderate protection factors of $\sim10^3$ to 10^4, indicative of exchange through sub-global fluctuations. In striking contrast, none of the amides in HI-1, HI-2, or H3 were measurably protected from exchange within the ~8 min dead time of this experimental approach. Thus the C-terminal inhibitory helices are significantly more stable than the N-terminal inhibitory helices and the DNA recognition helix.

Rapid proton-proton HX rate constants for Ets-1ΔN301, measured as magnetization transfer from water using the CLEANEX method, are also presented in Fig. 4*B*. To expand the number of amides showing detectable exchange by this approach, experiments were carried out at four pH values. Within the ETS domain, residues clustering near the DNA binding interface exhibited rapid HX with k_{ex} values ranging up to $\sim60\ s^{-1}$. These include Lys^{379}-Glu^{385}, forming the turn of the HTH motif, and Ala^{406}-Arg^{409} in the S3/S4 loop or wing. The low protection factors for these residues are consistent with their solvent exposure and high r.m.s.d. within the structural ensemble of Ets-1ΔN301, as well as with their flexibility detected by ^{15}N relaxation measurements. More strikingly, reliable k_{ex} values of ~1 to $2\ s^{-1}$ at pH 8.25, corresponding to protection factors of ~400, were measured for amides in helix H3. This indicates a significant degree of conformational fluctuations and limited local stability for the DNA recognition helix of Ets-1ΔN301. Interestingly, amides in H3 of the Fli-1 ETS domain also show little protection from HX (63), whereas in PU.1, amides in H3 exchange more slowly than those in the first helix of the HTH motif, H2 (59).

Residues throughout the N-terminal inhibitory sequence, but not the C-terminal inhibitory sequence, are characterized by relatively rapid HX. Amides located in the HI-1/HI-2 (Arg^{311}-Lys^{318}) and HI-2/H1 (Gly^{331}-Gln^{336}) loops underwent exchange with protection factors of only ~2–20. This corroborates structural and ^{15}N relaxation measurements, indicating that these regions of Ets-1ΔN301 are highly dynamic and readily solvent-exposed. More significantly, amides in HI-1 exchanged readily with water and exhibited a progressive decrease in k_{ex} values from the ends to the middle of this helix, indicative of fraying. HI-2 also showed measurable proton-proton HX, particularly toward its C-terminal end. The measured k_{ex} values, corresponding to average protection factors of only ~15 for HI-1 and ~75 for HI-2, demonstrate that, even in the absence of DNA, the N-terminal inhibitory helices of Ets-1ΔN301 are only marginally stable relative to their unfolded states (ΔG^{o}_{HX} ~1.6 kcal/mol and 2.6 kcal/mol, respectively, for unfolding). It is also noteworthy that, whereas in an isolated helix the N-terminal three amide protons are not involved in intrahelical hydrogen bonds and thus are expected to show little protection from HX, in the structure ensemble of Ets-1ΔN301, HI-1 abuts H4 such that the amide protons of Phe^{304} and Lys^{305} at the N terminus of HI-1 are positioned to hydrogen bond to carbonyl groups in H4. However, the low protection factors measured for these two residues indicate that such potential hydrogen bonds contribute little to the stability of HI-1 and its packing against H4. Taken together, these results support the hypothesis that helix HI-1, and possibly HI-2, are conformationally dynamic and poised to unfold as part of the allosteric mechanism of Ets-1 autoinhibition.

DISCUSSION

Structure of the Inhibitory Module—The NMR-derived structural ensemble of a partially-repressed Ets-1 fragment, Ets-1ΔN301, provides a complete view of the interactions between the ETS domain and inhibitory module. Four structurally coupled inhibitory helices, HI-1, HI-2, H4, and H5 pack intramolecularly with each other and with the first helix of the ETS domain (H1). This model is consistent with: (i) the role of H1 in both ETS domain DNA binding and autoinhibition (11); (ii) the previously determined secondary structure and amphipathic nature of the inhibitory helices (9); (iii) the hypothesized tertiary packing of these helices derived from the chemical shift differences between fully-repressed Ets-1ΔN280 and activated Ets-1ΔN331 (9); (iv) backbone amide ^{15}N relaxation measurements from this report indicating that Ets-1ΔN301 behaves as a well-folded globular protein; and (v) deletion and mutational analyses, including that of v-Ets, which establish the structural and functional coupling between the N- and C-terminal inhibitory sequences flanking the ETS domain (3–6,12). Furthermore, the ensemble of solution structures of monomeric Ets-1ΔN301 explains the intermolecular packing of HI-1 in the crystal structure of the three-dimensional domain-swapped Ets-1ΔN301 dimer (12). The ETS domain and the inhibitory module of both structures share similar features including the hydrophobic contacts between HI-1 and the remainder of the inhibitory module, as well as the tail-to-head alignment of H4 and HI-1. Predictably, the solution and crystalline state structures differ in the position of the flexible HI-1/HI-2 loop, which serves as a hinge between the two subunits of the crystalline dimer.

The architecture of the Ets-1ΔN301 ETS domain and C-terminal inhibitory helices also closely matches that found in the crystal structure of the ETS protein GABPα (15). GABPα interacts with a heterotypic partner, GABPβ, that itself does not bind DNA. Interestingly, the ankyrin repeats of GABPβ provide hydrophobic interactions, to helix H1 of the ETS domain and to helices C-terminal to this domain in GABPα, that

resemble those made by the N-terminal inhibitory sequence of Ets-1ΔN301. However, in contrast to a role in the negative regulation of Ets-1, within the context of the GABPα/β heterodimer, these contacts enhance DNA binding activity (64).

Dynamics and Stability of the Inhibitory Module—The dynamic measurements reported here describe a labile inhibitory module. The evidence for limited stability and flexibility of the N-terminal inhibitory helices is provided through three experimental avenues: ^{15}N relaxation, ^{15}N relaxation-dispersion, and amide HX studies. The findings are consistent with previous chymotrypsin and trypsin proteolysis studies of Ets-1ΔN280 (2, 3) and Ets-1ΔN301 (57)[4] demonstrating cleavage at residues in or adjacent to HI-1 (Phe^{304}, Tyr^{307}, Arg^{309}, Arg^{311}) and HI-2 (Leu^{326}, Tyr^{329}), even in the absence of DNA. Such cleavage is indicative of structural fluctuations, allowing access of the polypeptide chain to the active site cleft of the protease. These observations support the hypothesis that Ets-1 autoinhibition involves a marginally stable inhibitory module with helices HI-1, and possibly HI-2, undergoing a facile helix-coil transition.

Amide ^{15}N relaxation measurements revealed local backbone motions in HI-1, as well as in regions of Ets-1ΔN301 beyond this marginally stable helix. The HI-1/HI-2 loop exhibits sub-nanosecond conformational mobility, while the remainder of the inhibitory module is relatively well ordered on this time scale. However, relaxation-dispersion measurements indicate that HI-1 is undergoing intermediate millisecond-microsecond time scale motions leading to amide chemical shift exchange broadening (R_{ex} terms). Additional regions also show relaxation-dispersion properties indicative of intermediate time scale mobility, including HI-2, and to a lesser extent, H4 and H5 of the inhibitory module. Residues forming the DNA binding surface of ETS domain, specifically helix H1, H3, the HTH turn, and the S3/S4 loop, also display similar properties. We propose that the inhibitory module and helix H1, with which it directly interfaces, are in an equilibrium between different conformational states even in the absence of DNA. This conformational equilibrium may extend to the DNA binding interface of Ets-1 through van der Waals packing of residues in the ETS domain. Future studies will address whether these R_{ex} terms reflect fluctuations within a conformational ensemble sampled by the intact inhibitory module and/or excursions of the N-terminal inhibitory helices HI-1 and HI-2 and possibly the DNA recognition helix H3 to unfolded states detectable by HX measurements. Nevertheless, these findings are consistent with a growing body of evidence that internal motions of proteins on the millisecond-microsecond time scale are important for their allosteric regulation (65, 66).

Amide HX experiments complemented NMR relaxation measurements in providing a view of the local stability of the inhibitory module and ETS domain. Fast HX studies revealed that residues in helices HI-1 and HI-2 in Ets-1ΔN301 have amide proton exchange rates only ~15- and ~75-fold slower, respectively, than expected for a random coil polypeptide. Even lower protection from exchange is observed for the exposed amides in the intervening HI-1/HI-2 loop. Thus, the N-terminal inhibitory helices readily undergo local conformational fluctuations, allowing base-catalyzed hydrogen exchange with the water. In contrast, slower proton-deuterium HX measurements yielded protection factors of $\sim 10^3$ to 10^4 for amides in the C-terminal inhibitory helices H4 and H5, and $>10^6$ for those in H1 of the ETS domain. Therefore, helices H1, H4, and H5 appear to be a stable scaffold upon which the more labile helices HI-1 and HI-2 pack to form the inhibitory module. Indeed, in fully activated Ets-1ΔN331, which lacks the entire N-terminal inhibitory sequence, helices H1, H4, and H5 are folded (56).

Several plausible explanations for the limited stability of HI-1 and HI-2 can be garnered from consideration of the structure of Ets-1ΔN301. The hydrophobic interface between amphipathic helix HI-1 and the remainder of the N- and C-terminal inhibitory sequences buries only a modest amount of non-polar surface area (<800 Å^2). Furthermore, of the first 20 residues in Ets-1ΔN301, half have ionizable side chains, yielding a high charge density on HI-1 and the HI-1/HI-2 loop. In particular, this may lead to unfavorable (i,i+4) charge-charge interactions between Lys^{305}-Arg^{309} and Asp^{306}-Asp^{310} when these pairs of residues become aligned along helix HI-1 (67). The side chain carboxylate of Asp^{310} at the HI-1 C terminus might also repel the negative end of the helix macrodipole (68). In contrast to HI-1, the stability of the non-polar alanine-rich helix HI-2 may be limited by its packing across the relatively polar surface of helix H1, including the side chain of Gln^{339}.

Dynamics of the DNA Binding Interface—The dynamic studies of Ets-1ΔN301 also reveal a flexible DNA binding interface. As expected due to their surface exposure, the turn of the HTH motif and S3/S4 loop or wing exhibit high r.m.s.d. within the NMR-derived structure ensemble and elevated thermal B-values in the crystallographically derived structure of this protein, along with reduced S^2 order parameters and limited protection from amide HX. Consistent with this flexibility, crystallographic studies of Ets-1 show that the conformations of the HTH turn and S3/S4 loop change upon major groove binding by the recognition helix H3 in order to provide flanking contacts to the DNA phosphodiester backbone (12, 19). Surprisingly, H3 itself also exhibits significant conformational mobility as evident by HX protection factors of only ~400 and by millisecond-microsecond motions detected though relaxation-dispersion measurements. This flexibility, which is an emerging theme with many DNA-binding proteins (66, 69), could facilitate specific DNA recognition since alternative conformations of contact residues have been shown to play a role in target site selection by ETS domain proteins (19, 70).

Allosteric Mechanism of Ets-1 Autoinhibition—A combination of conformational and dynamic data extends the previously hypothesized allosteric model of Ets-1 autoinhibition. The NMR-derived structural ensemble of monomeric Ets-1ΔN301 confirms that the inhibitory module is distal from the HTH DNA binding interface of the ETS domain. This is consistent with previous thermodynamic and kinetic studies, which revealed that DNA binding by Ets-1 is neither sterically blocked nor modified in the number or nature of protein-DNA contacts made due to the presence of the inhibitory sequences (3, 71). Together with proteolysis studies, CD spectroscopic measurements, as well as crystallographic and NMR spectroscopic structural studies of Ets-1/DNA complexes, these data lead to an allosteric model of Ets-1 autoinhibition in which unfolding of at least helix HI-1 in the N-terminal inhibitory sequence accompanies DNA binding, while refolding of this helix favors complex dissociation (Fig. 5). Dynamic measurements by NMR relaxation and amide hydrogen exchange, combined with previous proteolysis studies (2, 3), provide two additional dimensions to this model: (i) HI-1 has low stability and thus is poised to unfold; and (ii) regions of the inhibitory module, as well as of the ETS domain, appear to undergo exchange between conformational states on a millisecond-microsecond time scale, even in the absence of DNA. These data also provide insights into the energetic coupling of DNA binding with the HI-1 helix-coil transition. Based on HX protection factors of ~15, ΔG^{o}_{HX} ~1.6 kcal/mol for the transient unfolding of HI-1 in DNA-free Ets-1ΔN301. This small energetic penalty is consist-

[4] I. Pot, unpublished data.

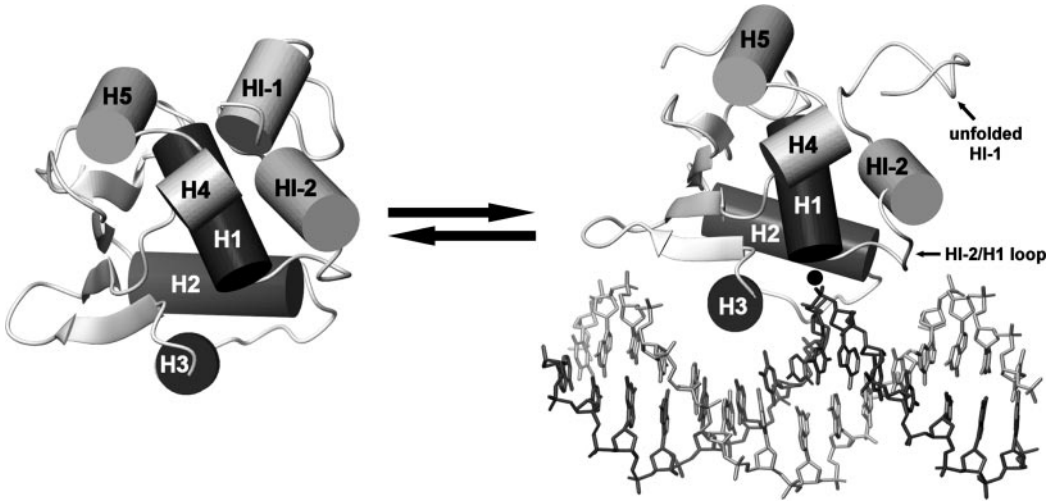

FIG. 5. **A model of the allosteric mechanism of autoinhibition in which the facile unfolding of helix HI-1 is coupled to DNA binding by the adjacent ETS domain.** Shown are the NMR-derived structure of free Ets-1ΔN301 and the crystallographically determined structure of Ets-1ΔN280 in complex with DNA (19). The helices of the ETS domain are indicated in *dark gray*, while those of the inhibitory module are displayed in *light gray*. Amide ^{15}N relaxation and HX data demonstrate that HI-1 is only marginally stable and thus poised to unfold. Formation of the intermolecular hydrogen bond between the amide of Leu^{337} and the DNA phosphodiester backbone (*black dot*) appears to require a shift in the position of the HI-2/HI loop, which could be linked with the unfolding of this inhibitory helix.

ent with $\Delta\Delta G^{o}_{bind} \sim 0.4$ kcal/mol corresponding to the ~2-fold inhibition of DNA binding by Ets-1ΔN301 relative to the fully activated truncation fragment, Ets-1ΔN331.

Based on its structural role in both the ETS domain and the inhibitory module, we have proposed that helix H1 is central to the allosteric mechanism of autoinhibition (11). This proposal is supported by several lines of evidence. X-ray crystallographic analyses demonstrated that H1 must be positioned precisely to form a hydrogen bond between the amide of Leu^{337} at its N terminus and the DNA phosphodiester backbone. This hydrogen bond is likely augmented by orienting the positive end of the macrodipole of this helix adjacent to the negatively charged nucleic acid backbone (12, 19). The importance of the interactions involving HI toward DNA binding and autoinhibition was confirmed by mutational analyses of both Ets-1ΔN280 and its target DNA (11).

Flexibility in both the ETS domain and autoinhibitory module appears to accommodate the structural changes that accompany DNA binding. The crystal structures of free Ets-1ΔN300 and DNA bound Ets-1ΔN280 are very similar, with the dramatic exception of HI-1 being domain-swapped or unfolded, respectively (12). However, important conformational changes between these species are detectable using a C^{α} difference distance matrix approach that is independent of the choice of co-ordinate superimposition (72). These changes can be divided into two categories, those that accommodate DNA binding, and those that affect the conformation of the inhibitory module. Exemplifying the former, the turn of the HTH motif and the loop between β-strands S3 and S4 shift to facilitate nucleic acid contacts. In the latter category, the relative positions of helix HI-2 and the HI-2/H1 loop change by over 1 Å with respect to the ETS domain. This perturbation is accompanied by pronounced alterations in the backbone conformation of the HI-2/H1 loop, as well as the disruption of a potential hydrogen bond between the side chains of Ser^{332} in this loop and Gln^{339} in helix H1. These observations suggest that, in order for helix H1 to precisely interact with DNA, the preceding HI-2/H1 loop must be shifted relative to its position in the free protein. This in turn would require the displacement of the non-polar alanine-rich helix HI-2 away from the DNA and across the relatively polar surface of H1 that is defined in part by Gln^{339}. Such a displacement would likely be coupled to a disruption of the hydrophobic packing of the N-terminal inhibitory region and thus linked with the unfolding of the marginally stable HI-1. Each of these categories of conformational change is consistent with regions of flexibility within Ets-1ΔN301 detected by ^{15}N relaxation and HX measurements

NMR measurements complement the insights gained from static Ets-1 structures and provide new dynamic views of the mechanism of autoinhibition. In addition to the limited stability of HI-1 and HI-2 detected by fast HX measurements, motions on the millisecond-microsecond time scale, leading to R_{ex} terms, were also detected for amides within both the inhibitory module and the ETS domain. A simple interpretation of these data is that DNA-free Ets-1ΔN301 is in conformational equilibrium that extends beyond fluctuations of the N-terminal inhibitory region. We speculate that this pre-existing equilibrium may be an additional feature of the allosteric coupling of DNA binding by the ETS domain with the helix-coil transition of the inhibitory module. For example, in addition to the postulated link between the unfolding of HI-1 and the precise positioning of H1 and the HI-2/H1 loop, it is possible that conformational mobility of the winged HTH motif of the ETS domain is required for high affinity DNA binding and that this mobility is coupled to the dynamic behavior of the inhibitory module. Consistent with studies in other systems, the millisecond-microsecond time scale of these motions appears to be a hallmark of protein regulatability (65, 66, 73). In the case of Ets-1, this regulation is versatile. Cellular conditions that trap an unfolded helix would result in activation of DNA binding, whereas those that limit the unfolding of this helix would result in increased inhibition. In this way, the N-terminal inhibitory elements, distinct from the more stable C-terminal helices, serve as the control point or effector of signals that regulate DNA binding affinity.

In summary, we have used NMR spectroscopy to characterize the structure and dynamics of a partially inhibited fragment of Ets-1. These studies provided the first description of the intramolecular packing of the inhibitory module, identified a potential conformational exchange equilibrium linked to the allosteric mechanism of autoinhibition, and defined the marginally stable nature of the N-terminal inhibitory helices. Together, these results establish a molecular framework necessary for understanding how protein partnerships, post-

translational modifications, or mutations alter the stability of the inhibitory module and thereby regulate the affinity of Ets-1 for its target promoter sequences.

Acknowledgments—We thank Wing-Yiu (James) Choy, Gregory Connelly, Lisa Gentile, Marc Gillespie, Lewis Kay, Oscar Millet, Ranjith Muhandiram, Frans Mulder, and Philip Webster for technical assistance. Instrument support was provided by the Government of Canada's Network of Centres of Excellence Program supported by the Canadian Institutes of Health Research (CIHR) and the Natural Sciences and Engineering Research Council (NSERC) through the Protein Engineering Network of Centres of Excellence (PENCE, Inc.).

REFERENCES

1. Pufall, M. A., and Graves, B. J. (2002) *Annu. Rev. Cell Dev. Biol.* **18,** 421–462
2. Petersen, J. M., Skalicky, J. J., Donaldson, L. W., McIntosh, L. P., Alber, T., and Graves, B. J. (1995) *Science* **269,** 1866–1869
3. Jonsen, M. D., Petersen, J. M., Xu, Q., and Graves, B. J. (1996) *Mol. Cell. Biol.* **16,** 2065–2073
4. Hagman, J., and Grosschedl, R. (1992) *Proc. Natl. Acad. Sci. U. S. A.* **89,** 8889–8893
5. Hahn, S. L., and Wasylyk, B. (1994) *Oncogene* **9,** 2499–2512
6. Fisher, R. J., Fivash, M., Casas-Finet, J., Erickson, J. W., Kondoh, A., Bladen, S. V., Fisher, C., Watson, D. K., and Papas, T. (1994) *Prot. Sci.* **3,** 257–266
7. Goetz, T. L., Gu, T.-L., Speck, N. A., and Graves, B. J. (2000) *Mol. Cell. Biol.* **20,** 81–90
8. Cowley, D. O., and Graves, B. J. (2000) *Genes Dev.* **14,** 366–376
9. Skalicky, J. J., Donaldson, L. W., Petersen, J. M., Graves, B. J., and McIntosh, L. P. (1996) *Prot. Sci.* **5,** 296–309
10. Donaldson, L. W., Petersen, J. M., Graves, B. J., and McIntosh, L. P. (1996) *EMBO J.* **15,** 125–134
11. Wang, H., McIntosh, L. P., and Graves, B. J. (2002) *J. Biol. Chem.* **277,** 2225–2233
12. Garvie, C. W., Pufall, M. A., Graves, B. J., and Wolberger, C. (2002) *J. Biol. Chem.* **277,** 45529–45536
13. Liu, Y., and Eisenberg, D. (2002) *Protein Science* **11,** 1285–1299
14. Kodandapani, R., Pio, F., Ni, C.-Z., Piccialli, G., Klemsz, M., McKercher, S., Maki, R. A., and Ely, K. R. (1996) *Nature* **380,** 456–460
15. Batchelor, A. H., Piper, D. E., de la Brousse, F. C., McKnight, S. L., and Wolberger, C. (1998) *Science* **279,** 1037–1041
16. Mo, Y., Vaessen, B., Johnston, K., and Marmorstein, R. (1998) *Mol. Cell* **2,** 201–212
17. Mo, Y., Vaessen, B., Johnston, K., and Marmorstein, R. (2000) *Nat. Struct. Biol.* **7,** 292–297
18. Graves, B. J., Cowley, D. O., Goetz, T. L., Petersen, J. M., Jonsen, M. D., and Gillespie, M. E. (1998) *CSH Symp. Quant. Biol.* **63,** 621–629
19. Garvie, C. W., Hagman, J., and Wolberger, C. (2001) *Mol. Cell* **8,** 1267–1276
20. Donaldson, L. W., Petersen, J. M., Graves, B. J., and McIntosh, L. P. (1994) *Biochemistry* **33,** 13509–13516
21. Szyperski, T., Neri, D., Leiting, B., Otting, G., and Wüthrich, K. (1992) *J. Biolmol. NMR* **2,** 323–334
22. McIntosh, L. P., and Dahlquist, F. W. (1990) *Q. Rev. Biophys.* **23,** 1–38
23. Delaglio, F., Grzesiek, S., Vuister, G. W., Zhu, G., Pfeifer, J., and Bax, A. (1995) *J. Biomol. NMR* **6,** 277–293
24. Goddard, T. D., and Kneeler, D. G. (1999) *Sparky* 3rd Ed., San Francisco, CA
25. Sattler, M., Schleucher, J., and Griesinger, C. (1999) *Progr. NMR Spectros.* **34,** 93–158
26. McIntosh, L. P., Brun, E., and Kay, L. E. (1997) *J. Biomol. NMR* **9,** 306–312
27. Brünger, A. T., Adams, P. D., Clore, G. M., DeLano, W. L., Gros, P., Grosse-Kunstleve, R. W., Jiang, J.-S., Kuszewski, J., Nilges, M., Pannu, N. S., Read, R. J., Rice, L. M., Simonson, T., and Warren, G. L. (1998) *Acta Crystallogr. Sect. D* **54**, 905–921
28. Linge, J. P., Habeck, M., Rieping, W., and Nilges, M. (2003) *Bioinformatics* **19,** 315–316
29. Zwahlen, C., Gardner, K. H., Sarma, S. P., Horita, D. A., Byrd, R. A., and Kay, L. E. (1998) *J. Am. Chem. Soc.* **120,** 7617–7625
30. Cornilescu, G., Delaglio, F., and Bax, A. (1999) *J. Biomol. NMR* **13,** 289–302
31. Vuister, G. W., Wang, A. C., and Bax, A. (1993) *J. Am. Chem. Soc.* **115,** 5334–5335
32. Schubert, M., Labudde, D., Oschkinat, H., and Schmieder, P. (2002) *J. Biomol. NMR* **24,** 149–154
33. Ishii, Y., Markus, M. A., and Tycko, R. (2001) *J. Biomol. NMR* **21,** 141–151
34. Chou, J. J., Gaemers, S., Howder, B., Louis, J. M., and Bax, A. (2001) *J. Biomol. NMR* **21,** 377–382
35. Ottiger, M., Delaglio, F., and Bax, A. (1998) *J. Magn. Reson.* **131,** 373–378
36. Clore, G. M., Gronenborn, A. M., and Bax, A. (1998) *J. Mag. Res.* **133,** 216–221
37. Schweiters, C. D., and Clore, G. M. (2001) *J. Mag. Res.* **149,** 239–244
38. Koradi, R., Billeter, M., and Wüthrich, K. (1996) *J. Mol. Graphics* **14,** 51–55
39. Laskowski, R. A., Rullmann, J. A. C., MacArthur, M. W., Kaptein, R., and Thornton, J. M. (1996) *J. Biomol. NMR* **8,** 477–486
40. Hutchinson, E. G., and Thornton, J. M. (1996) *Prot. Sci.* **5,** 212–220
41. Willard, L., Ranjan, A., Zhang, H., Monzavi, H., Boyko, R. F., Sykes, B. D., and Wishart, D. S. (2003) *Nucleic Acids Res.* **31,** 3316–3319
42. Farrow, N. A., Muhandiram, R., Singer, A. U., Pascal, S. M., Kay, C. M., Gish, G., Shoelson, S. E., Pawson, T., Forman-Kay, J. D., and Kay, L. E. (1994) *Biochemistry* **33,** 5984–6003
43. Lipari, G., and Szabo, A. (1982) *J. Am. Chem. Soc.* **104,** 4546–4558
44. Kay, L. E., Torchia, D. A., and Bax, A. (1989) *Biochemistry* **28,** 8972–8979
45. Mandel, A. M., Akke, M., and Palmer, A. G. (1995) *J. Mol. Biol.* **246,** 144–163
46. Palmer, A. G., III. (1998) *CurveFit* 1.22 Ed., Columbia University, New York
47. Dosset, P., Hus, J.-C., Blackledge, M., and Marion, D. (2000) *J. Biomol. NMR* **16,** 23–28
48. Mulder, F. A. A., Skrynnikov, N. R., Hon, B., Dahlquist, F. W., and Kay, L. E. (2001) *J. Am. Chem. Soc.* **123,** 967–975
49. Millet, O., Loria, J. P., Kroenke, C. D., Pons, M., and Palmer, A. G. I. (2000) *J. Am. Chem. Soc.* **122,** 2867–2877
50. Connelly, G. P., and McIntosh, L. P. (1998) *Biochemistry* **37,** 1810–1818
51. Hwang, T.-L., van Zijl, P. C. M., and Mori, S. (1998) *J. Biomol. NMR* **11,** 221–226
52. Zhang, Y.-Z. (1995) *Protein and Peptide Structure and Interactions Studied by Hydrogen Exchange and NMR*. Ph.D. thesis, University of Pennsylvania, Philadelphia
53. Bai, Y., Milne, J. S., Mayne, L., and Englander, S. W. (1993) *Proteins* **17,** 75–86
54. Connelly, G. P., Bai, Y., Jeng, M. F., and Englander, S. W. (1993) *Proteins* **17,** 87–92
55. Werner, M. H., Clore, G. M., Fisher, C. L., Fisher, R. J., Trinh, L., Shiloach, J., and Gronenborn, A. M. (1997) *J. Biomol. NMR* **10,** 317–328
56. Donaldson, L. W. (1996) *Structural Studies of the ETS Domain.* Ph.D. thesis, University of British Columbia, Vancouver
57. Jonsen, M. D. (1999) *Autoinhibition of DNA Binding in the Transcription Factor Ets-1: A Mechanistic and Structural Study*, Ph.D. thesis, University of Utah, Salt Lake City
58. Daragan, V. A., and Mayo, K. H. (1997) *Prog. Nucl. Magn. Reson. Spect.* **31,** 63–105
59. Jia, X., Lee, L. K., Light, J., Palmer, A. G. I., and Assa-Munt, N. (1999) *J. Mol. Biol.* **292,** 1083–1093
60. Loria, J. P., Rance, M., and Palmer, A. G. I. (1999) *J. Am. Chem. Soc.* **121,** 2331–2332
61. Englander, S. W., Sosnick, T. R., Engalnder, J. J., and Mayne, L. (1996) *Curr. Opin. Struct. Biol.* **6,** 18–23
62. Englander, S. W., and Kallenbach, N. R. (1984) *Q. Rev. Biophys.* **16,** 521–655
63. Liang, H., Olejniczak, E., Mao, X., Nettesheim, D., Yu, L., Thompson, C., and Fesik, S. (1994) *Proc. Natl. Acad. Sci. U. S. A.* **91,** 11655–11659
64. Thompson, C. C., Brown, T. A., and McKnight, S. L. (1991) *Science* **253,** 762–768
65. Kern, D., and Zuiderweg, E. R. P. (2003) *Curr. Opin. Struct. Biol.* **13,** 748–757
66. Yan, J., Liu, Y., Lukasik, S. M., Speck, N. A., and Bushweller, J. H. (2004) *Nature Struct. Mol. Biol.* **11,** 901–906
67. Marqusee, S., and Baldwin, R. L. (1987) *Proc. Natl. Acad. Sci. U. S. A.* **84,** 8898–8902
68. Chakrabartty, A., and Baldwin, R. L. (1995) *Adv. Prot. Chem.* **46,** 141–175
69. Kalodimos, C. G., Biris, N., Bonvin, A. M. J. J., LLevandoski, M. M., Guennuegues, M., Boelens, R., and Kaptein, R. (2004) *Science* **305,** 386–389
70. Pufall, M. A., and Graves, B. J. (2002) *Structure* (*Camb*) **10,** 11–14
71. Nye, J. A., Petersen, J. M., Gunther, C. V., Jonsen, M. D., and Graves, B. J. (1992) *Genes Dev.* **6,** 975–990
72. Richards, F. M., and Kundrot, C. E. (1988) *Proteins* **3,** 71–84
73. Wolf-Watz, M., Thai, V., Henzler-Wildman, K., Hadjipavlou, G., Eisenmesser, E. Z., and Kern, D. (2004) *Nat. Struct. Mol. Biol.*, **11,** 945–949
74. Slupsky, C. M., Gentile, L. N., Donaldson, L. W., Mackereth, C. D., Seidel, J. J., Graves, B. J., and McIntosh, L. P. (1998) *Proc. Natl. Acad. Sci. U. S. A.* **95,** 12129–12134
75. Seidel, J. J., and Graves, B. J. (2002) *Genes Dev.* **16,** 127–137